Available online at www.sciencedirect.com
SCIENCE DIRECT®
Journal of Nuclear Materials 320 (2003) 280–291
journal of nuclear materials
www.elsevier.com/locate/jnucmat

Recrystallization of almost fully amorphous zircon under hydrothermal conditions: An infrared spectroscopic study

Thorsten Geisler [a,b,*], Ming Zhang [b], Ekhard K.H. Salje [b]

[a] *Institut für Mineralogie, University of Münster, Corrensstraße 24, D-48149 Münster, Germany*
[b] *Department of Earth Sciences, University of Cambridge, Downing Street, Cambridge CB2 3EQ, UK*

Received 9 January 2003; accepted 13 March 2003

Abstract

Hydrothermal experiments were carried out with powder from an almost fully amorphous, natural zircon under various *P–T–t* conditions mainly in a 0.1 N HCl solution. Powder infrared spectroscopic measurements on the experimental products reveal that first structural changes occurred at a fluid temperature as low as 75 °C. Significant recrystallization started at 200 °C, as indicated by an increase in the absorption intensity of the zircon fundamental IR bands and the formation of sharp OH stretching bands at 3385 and 3420 cm^{-1}. Although the powder has fully reacted at 400 °C, the zircon fundamental absorption bands are not fully recovered, indicating the occurrence of significant amounts of amorphous remnants. The experimental results in neutral to acidic solutions are consistent with the idea that water (H^+ and possibly H_2O) diffuses into the amorphous network where it 'catalyses' solid state recrystallization. During this process, Zr and Si were leached from the amorphous network.

1. Introduction

Zircon ($ZrSiO_4$) has been proposed as a durable immobilization phase for weapons-grade plutonium due to its capability to structurally accept several weight percent of Pu at the Zr site [1,2]. Polycrystalline zircon containing 10 wt% Pu has been synthesized [3]. Recently, Pu-doped single crystals have been synthesized containing up to 1.4 wt% Pu [4]. However, for the application of zircon as a nuclear waste form it is crucial to understand the alteration of self-irradiated zircon in aqueous solutions. Numerous studies on natural zircon samples reveal that zircon is enigmatic in its resistance to fluid attack. Whereas zircon is known to survive and remain chemically closed under extreme geological conditions [2], discordant U–Pb ages have been found in zircon crystals from low *P–T* environments [5,6]. This discrepancy can partially be explained by the process of metamictization, which was found to decrease the stability of zircon against aqueous solutions [7,8]. During metamictisation U- and Th-bearing zircon undergoes a transition from a crystalline to an almost fully amorphous state as a result of self-irradiation through radioactive decay of U and Th [9–11]. The heavy recoil atom produced during a radioactive α-decay event permanently displaces about 4000 atoms in zircon [12], whereas only several hundred atoms are displaced by the alpha particle [10]. In the initial state of metamictization the zircon structure consists of isolated aperiodic domains inside a crystalline but slightly disordered structure, whereas the final (metamict) state of radiation damage is characterized by highly distorted, nano-crystalline remnants, which are randomly located in an amorphous matrix [9–11]. Infrared and NMR investigations have shown that the amorphous phase is polymerized to some extent [12,13]. However, the present knowledge about the short- and medium-range order in

* Corresponding author. Address: Institut für Mineralogie, University of Münster, Corrensstraße 24, D-48149 Münster, Germany. Tel.: +49-251-833-3450; fax: +49-251-833-8397.
E-mail addresses: tgeisler@nwz.uni-muenster.de, t.geisler-wierwille@t-online.de (T. Geisler).

0022-3115/03/$ - see front matter © 2003 Elsevier B.V. All rights reserved.
doi:10.1016/S0022-3115(03)00187-9

amorphous zircon is very limited, which, however, would be important to understanding aqueous alteration processes on the atomic scale.

Previous dry annealing experiments with partially metamict zircon samples have revealed that disordered crystalline remnants start to preferentially recover defects across the basal plane with an apparent activation energy in the order of 2.0–2.5 eV [14]. The amorphous regions epitaxially recrystallize around seeds of crystalline remnants at temperatures in excess of 1000 K under laboratory time scales, which is reflected by experimentally determined activation energies of about 3.8 eV [14,15], 3.6 eV [16], and 3.3 eV obtained under ion-beam irradiation conditions [17]. Defects that are responsible for a residual expansion of the *c*-axis in partially metamict zircon after almost complete annealing of the *a*-axis are stable up to high temperatures, as mirrored by a high activation energy in the order of 6–8 eV [15]. In heavily damaged crystals, the main recrystallization of amorphous $ZrSiO_4$ occurs at temperatures between 1400 and 1500 K after the amorphous material was partially decomposed into ZrO_2 and SiO_2 [10,18–20]. The activation energies of such a two-stage bulk thermal recrystallization process were determined to be 5.1 and 6.6 eV [3,18]. Compared with dry annealing experiments, metamict zircon recovers its crystallinity with a reduced activation energy under the influence of an aqueous phase, which has already been reported by Mumpton and Roy [21]. Recently, Geisler and coworkers were able to show that thermal annealing of partially metamict zircon under hydrothermal conditions produces rims of recrystallized zircon around apparently unreacted zircon, which were formed behind sharp reaction fronts [8,22,23]. Such a situation could in principal be produced by a dissolution–reprecipitation mechanism [24]. However, Geisler and coworkers [21,22] have shown that the reactions rims were formed by diffusion-driven ion exchange reactions, where water catalyzes structural recovery processes, including solid state recrystallization of the amorphous phase. Evidence for this model are, e.g., (1) diffusion-like concentration profiles of solute and solvent cations, (2) the formation of distinct zones or periodic ring patterns, indicative of diffusion–reaction processes, (3) retention of radiogenic Pb in the reaction rims and (4) the fact that the reaction zones do not consist of fully ordered, crystalline zircon, but show intermediate structural states also observed in dry annealing experiments, which would not be expected if the reaction is controlled by a coupled dissolution–reprecipitation process [21,22].

The objective of the present study was to systematically investigate recrystallization of amorphous zircon under different hydrothermal *P–T–t* and pH conditions. We used powder infrared spectroscopy to monitor the hydrothermal alteration of a heavily damaged zircon since this technique is sensitive to detect small structural alterations in the amorphous as well as in the crystalline network. Additional information was gained from FT-Raman spectroscopy and scanning electron microscopy.

2. Experimental procedures

The starting material for the experiments was a heavily metamict, green, gem-type, alluvial zircon crystal (HZ7) from Sri Lanka. The zircon crystal contains Hf and U as major impurities and has most likely not suffered any hydrothermal alteration in its geological history, as indicated by low Ca or Al concentrations (Table 1). High concentrations of Ca and Al in natural metamict zircon crystals were found to be indicators of hydrothermal alteration [6,25]. The amount of crystalline remnants is in the order of less than 5% as estimated from the α-decay dose given in Table 1 and the calibration given by Ríos and coworkers [26]. Aside from the powder infrared measurement of the untreated sample shown in Fig. 1, we also carried out ^{29}Si NMR, Raman and X-ray diffraction measurements (not shown), which additionally confirm the heavily metamict character of the sample.

The hydrothermal experiments were performed in gold capsules of 4 cm length, which were positioned in the hot spot of standard cold seal pressure vessels. The temperature and pressure were constant and accurate within 5 °C and 0.05 kbar, respectively. The gold capsules were weighed before and after the experiments to check for leakage. For each experiment about 100 mg fluid was added to 6–10 mg zircon powder. Secondary electron microscopic imaging of the powder revealed that the grain size was below ≈50 μm. In some experiments

Table 1
Chemical composition of the starting zircon HZ7, as determined by electron microprobe measurements, and the α-decay dose, *D* (α-decays g^{-1}), given for an age of 570 Ma

Oxide	wt%	±2σ
ZrO_2	64.35	±0.24
SiO_2	30.82	±0.10
HfO_2	1.90	±0.12
Y_2O_3	0.10	±0.06
P_2O_5	0.08	±0.02
UO_2	0.62	±0.08
ThO_2	0.04	±0.01
Yb_2O_3	0.09	±0.02
Al_2O_3	<0.005	
CaO	<0.006	
Total	98.00	
D	$(11.0 \pm 1.5) \times 10^{18}$	

The given errors were estimated from ten single measurements.

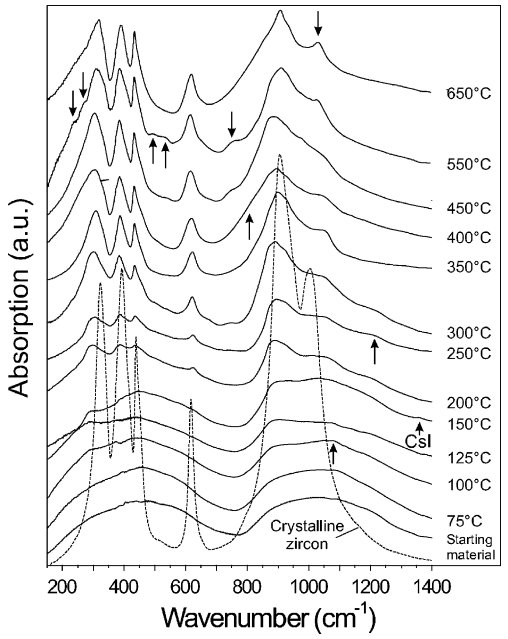

Fig. 1. Stack plot of powder IR absorption spectra between 150 and 1400 cm^{-1} of heavily metamict zircon treated under different temperatures between 75 and 650 °C in a 0.1 N HCl solution for 195 h at 1 kbar fluid pressure. A spectrum from the starting material and a crystalline reference sample is shown for comparison. Arrows point to new bands, which do not belong to zircon.

we further added larger grains (≃500 μm), which were mounted and polished after the experiments for backscattered electron (BSE) imaging. Four series of hydrothermal experiments were designed to study the influence of fluid temperature, pressure, experimental duration, and solution pH on the alteration of sample HZ7 (Table 2). However, a limited amount of sample material allowed studying the dependence of the zircon–fluid interaction on the experimental duration, pressure and pH only at a single temperature.

The conventional pellet technique was used to measure the far infrared (FIR) and mid infrared (MIR) absorption of the starting material and the experimental products. For this, one part of the powder was thoroughly mixed with 300 parts of dry CsI. 300 mg of this mixture were used to press a 13 mm disc-shaped pellet under vacuum and room temperature. The same pellet was measured in vacuum for both FIR and MIR regions with a Bruker IFS 113v and a Bruker IFS 66v spectrometer, respectively, within 12 h after its creation. A DTGS detector, coupled with a KBr beamsplitter and a Globar source, was used to record the spectra between 450 and 5000 cm^{-1}, whereas a DTGS detector with a polyethylene window, coupled with a mercury lamp and a 3.5 μm Mylar beamsplitter, was used to for the frequency region between 150 and 700 cm^{-1}. The spectral resolution was 2 cm^{-1}. The possible experimental errors that may affect IR analysis of powder absorption spectra have already been discussed by Zhang et al. [27].

Additional Raman measurements on the hydrothermally treated powders were carried out with a Bruker FRA106 FT-Raman accessory attached to the Bruker IFS 66v spectrometer. The Raman emission was excited with radiation of 1064 nm from an Nd:YAG laser with a 350 mW output. A liquid-nitrogen-cooled, high sensitivity Ge detector was used and the spectra were recorded with the maximum laser power in a back scattering geometry. The focused beam was about 200 μm in size and the spectra were accumulated over several hours. The resolution of the spectra was 2 cm^{-1}.

The most suitable band to quantitatively study the dependence of recrystallization on the fluid temperature is the zircon O–Si–O bending mode near 614 cm^{-1}. Before we carried out a least-squares peak fitting procedure, we removed a linear background between the lowest absorption at both sides of the peak. The remaining profile was often composed of the zircon bending mode and a shoulder at the high frequency side near 655 cm^{-1}. In these cases, the profiles had to be deconvoluted with two Gauss or Lorentz functions. In the experiment with a 3N HCl solution at 200 °C, we had also to consider a further contribution located at the low frequency side of the O–Si–O bending mode. The error associated with this fitting procedure was estimated to be less than ±2 cm^{-1} and less than ±0.5 in the peak position and the integrated absorption, respectively.

Table 2
Experimental conditions

Experimental series	T (°C)	P (kbar)	t (h)	Fluid composition
A	75–650	1.0	195	0.1 N HCl
B	400	0.5–2.5	51	0.1 N HCl
C	200	1.0	195	3.0 N HCl/0.1 N HCl/H_2O 0.1 N KOH/3.0 N KOH
D	400	1.0	3–195	0.1 N HCl

3. Results

3.1. Effect of fluid temperature

The powder absorption spectra of samples, which were hydrothermally treated 195 h at different temperatures between 75 and 650 °C under isobaric conditions (1 kbar fluid pressure) in a 0.1 N HCl solution (series A in Table 2), are shown in Fig. 1 in comparison with a spectrum of a crystalline zircon and the starting material. The IR spectrum of the starting material reflects a wide dispersal of vibrational states, which is characteristic of an amorphous network. Heavily damaged zircon such as sample HZ7 is characterized by additional broad absorption signals centered near 520, 680 and 1100 cm^{-1} [13]. However, a further broad signal appears near 1200 cm^{-1} in the spectrum of the starting material. The powder IR absorption spectrum from the crystalline zircon is characterized by sharp bands representing $v_3(SiO_4)$ stretching vibrations between 800 and 1100 cm^{-1} (i.e., the E_u mode at 903 cm^{-1} and A_{2u} mode at 1000 cm^{-1}), $v_4(SiO_4)$ bending vibrations near 434 and 612 cm^{-1} as well as external IR modes below 400 cm^{-1} [28].

The hydrothermally treated samples show gradual spectral changes with increasing fluid temperature (Fig. 1). With increasing temperature the absorption signals increase due to the zircon fundamental vibrations. It is evident that the most significant structural changes occurred at fluid temperatures higher than 200 °C. However, structural changes, which occurred in the experiments below 200 °C, are more evident in the difference spectra shown in Fig. 2. The difference spectra were obtained by subtracting the spectrum of the starting zircon from those of the experimental products. They clearly show that first spectral changes in the frequency range of zircon fundamental vibrations are already visible in the spectrum of the run product from the 75 °C experiment. The absorption maximum around 880 cm^{-1} increases with increasing fluid temperature and its position shifts from about 850 at 75 °C to 880 cm^{-1} at 200 °C. Note also that first small changes in the zircon O–Si–O bending frequency region around 614 cm^{-1} can already be detected in the difference spectrum of the 100 °C experiment. At temperatures higher than 150 °C the absorption intensity of the zircon fundamental modes continuously increases, indicating significant formation of crystalline $ZrSiO_4$. The temperature dependence of the absorption and the peak position of the $v_4(SiO_4)$ bending mode near 614 cm^{-1} is quantitatively shown in Fig. 3. Note that with increasing fluid temperature not only the absorption continuously increases (Fig. 3(a)), but that also frequency shifts to lower frequencies (Fig. 3(b)). A rapid increase of the absorption can be seen between 250 and 300 °C, whereas the frequency evolves linearly and gradually with increasing

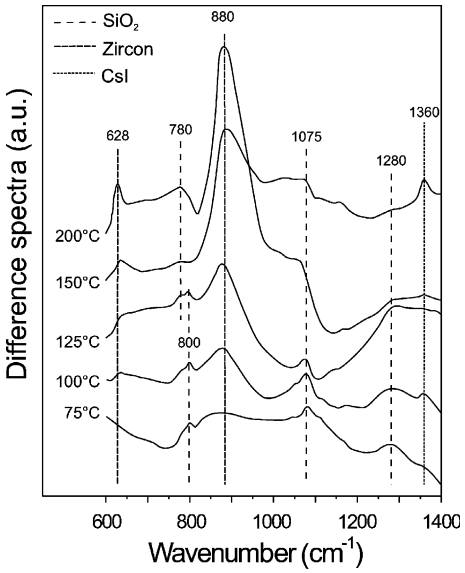

Fig. 2. Stacked difference spectra of heavily metamict zircon treated under different temperatures between 75 and 200 °C in a 0.1 N HCl solution for 195 h at 1 kbar fluid pressure after removing the spectrum of the starting material. Stippled lines mark those signals, which belong to zircon and silica fundamental vibrations. The origin of the signal near 1360 cm^{-1} is due to CsI.

temperature towards the value of crystalline zircon, which is almost reached at 450 °C (Fig. 3(b)). Also the absorption seems to reach saturation at 450 °C, although the fundamental zircon spectral features are still significant broader and less intense than those seen in crystalline zircon (Fig. 1), which indicates that a significant fraction of amorphous zircon still remains in the run products. Quantitatively, this means that the integrated absorption intensity of the bending mode near 614 cm^{-1} measured on the run product of the 650 °C experiment reaches only about 50% of the intensity determined for the crystalline reference zircon shown in Fig. 1.

A close look at the spectra in Fig. 1 further reveals new absorption signals centered around 220, 270, 490, 530, 800, 1080, 1280 and 1360 cm^{-1}, which do not belong to zircon fundamental vibrations. The band at 1360 cm^{-1} seen in some spectra can be assigned to CsI. The observed frequencies of the other bands are summarized in Table 3 for each experiment. With the exception of the signal between 1000 and 1100 cm^{-1}, which can be detected in all experiments, the occurrence of the other signals is not systematic. The signals near 220, 270 and 490 cm^{-1}, which can only be detected in the 550 °C experiment, can confidently be assigned to monoclinic ZrO_2 (m-ZrO_2) [29,30]. This is confirmed by Raman spectroscopic measurements on the run product from the same experiment (Fig. 4). Most additional Raman bands, i.e. those which do not reflect zircon fundamental

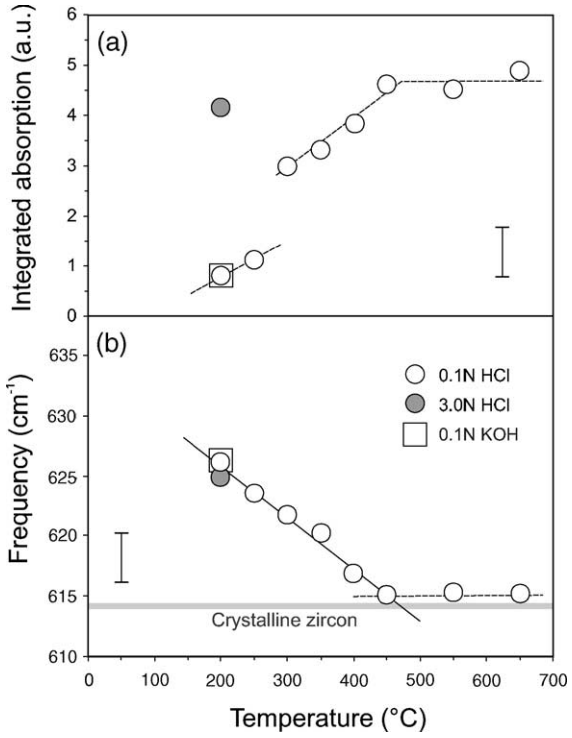

Fig. 3. (a) Integrated absorption and (b) the frequency of the zircon O–Si–O bending mode near 614 cm^{-1} for isochronal (195 h) experiments in a 0.1 N HCl, a 3.0 N HCl, and a 0.1 N KOH solution at 1 kbar fluid pressure as a function of fluid temperature. The solid line in (b) represents the best-fit line, whereas the stippled lines are guides to the eye only.

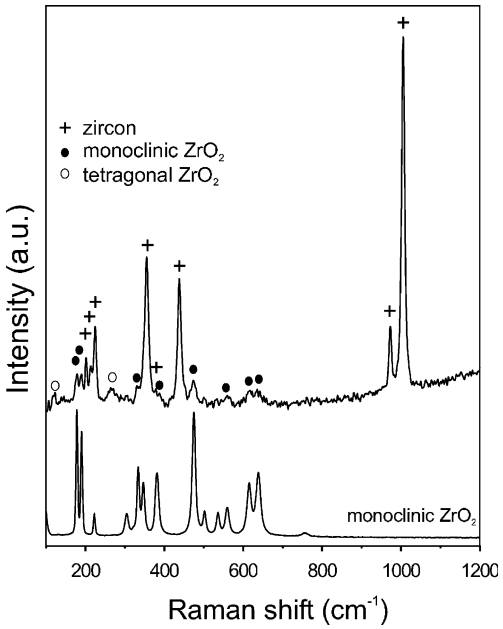

Fig. 4. FT-Raman spectrum between 100 and 1200 cm^{-1} of heavily metamict zircon treated at 550 °C in a 0.1 N HCl solution for 195 h at 1 kbar fluid pressure. A spectrum of synthetic monoclinic ZrO_2 is shown for comparison (lower spectrum). Note the occurrence of fundamental bands of monoclinic and tetragonal ZrO_2.

vibrations, match well with those obtained from commercial m-ZrO_2 (Alfa, 99.978%) (bottom spectra in Fig. 4) and a Raman spectrum of m-ZrO_2 reported in [31]. Further Raman bands centered near 120 and 265 cm^{-1} also indicate the presence of tetragonal ZrO_2 (t-ZrO_2). Note that tetragonal ZrO_2 has IR active modes at 436 and 363 cm^{-1} [29,30], which are hidden below the $v_4(SiO_4)$ bending vibration near 434 cm^{-1} and the lattice modes below 400 cm^{-1}. A further t-ZrO_2 infrared-active band occurs near 158 cm^{-1}, which, however, is weak. The occurrence of m-ZrO_2 in other run products from experiments at temperatures of 400 °C and higher is further indicated by a broad shoulder at the low frequency side of the IR lattice mode near 310 cm^{-1} (Fig. 1) and scanning electron microscope (SEM) observations (Fig. 5(d)).

Table 3
New infrared modes and their assignment (band frequency, cm^{-1}) after hydrothermal treatment of sample HZ7 at different temperatures in 0.1 N HCl for 195 h at 1 kbar

	Temperature (°C)											
	75	100	125	150	200	250	300	350	400	450	550[a]	650
m-ZrO_2	–	–	–	–	–	–	–	–	–	–	240	–
	–	–	–	–	–	–	–	–	*250*	*250*	274	*250*
	–	–	–	–	–	–	–	–	–	–	498	–
SiO_2	800	794	789	–	779	766	748	*770*	*800*	–	757	*800*
	1083	1079	1077	1076	1066	1060	1051	1051	1043	–	1026	1029
	–	–	–	1200[b]	1200[b]	1210[b]	–	–	–	–	–	–
	1280	1283	1285	–	–	–	–	–	–	–	–	–

The italicized values represent the approximate center of a broad signal.
[a] The origin of a further band near 530 cm^{-1} (Fig. 1) in this experiment is not known.
[b] This signal is also detectable in the starting material and thus not visible in the difference spectra of Fig. 2.

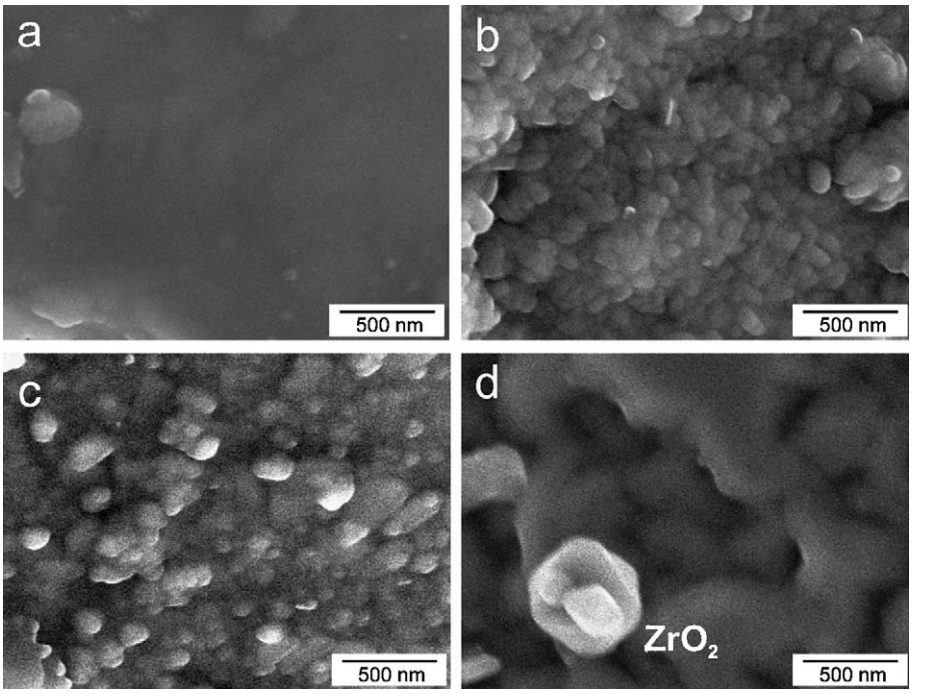

Fig. 5. SEM images of the surface of (a) a grain from the starting material, and grains hydrothermally treated at (b) 150 °C, (c) 300 °C and (d) at 650 °C in a 0.1 N HCl for 195 h at 1 kbar fluid pressure. Note the occurrence of silica spherules (b, c) and ZrO_2 crystals (d) on the surface of the grains and the porous structure, which can clearly be seen in (d).

SEM images of the grain surfaces further show the formation of silica spherules at the zircon–solution reaction interface (Fig. 5), which are similar to those seen on the surface of experimentally altered silicate glass [31]. Especially in the low-temperature experiment, the observed frequency of the modes near 800 cm^{-1} and between 1000 and 1100 cm^{-1} match well with those observed in amorphous, porous and colloidal silica, where these modes represent the O–Si–O bending and the asymmetrical Si–O stretching vibration, respectively [32–35]. The remaining IR band near 1280 cm^{-1}, seen in the low-temperature experiments (Table 3), may belong to porous silica, which often shows a high-frequency shoulder between 1150 and 1250 cm^{-1} [32]. The sharpness of the bands indicates crystalline silica, whereas the fact that SiO_2 could not be detected in the Raman spectrum (Fig. 4) points to the existence of amorphous silica rather than to a crystalline SiO_2 polymorph. Although it is impossible to confidently determine the structural state of the silica phase, there is no doubt that silica was formed during the experiments.

3.2. Effect of fluid pressure

Isothermal experiments at 400 °C were carried out at fluid pressures of 0.5, 1.0, 1.5 and 2.5 kbar with a 0.1 N HCl for 51 h (series B in Table 2). Fig. 6(a) shows the absorption spectra of run products from these experiments, which demonstrate that there is no significant effect of pressure up to 2.5 kbar on the absorption intensity and peak position of the zircon fundamental modes. The only pressure effect is seen in run products of the 2.5 kbar experiment. Here two sharp new modes can be detected at 1049 and 1087 cm^{-1}, whereas a single mode centered near 1050 cm^{-1} occurs in the spectra from the experiments at lower fluid pressure. Despite this difference, the new bands at 1049 and 1087 cm^{-1} can be assigned to SiO_2, which, however, must have a different structure at a fluid pressure of 2.5 kbar. The occurrence of m-ZrO_2 at all pressures is again indicated by a shoulder at the low frequency side of the zircon IR lattice mode near 310 cm^{-1}.

3.3. Effect of solution pH

To study the dependence of the hydrothermal alteration of heavily metamict zircon on the solution pH, we carried out four isothermal (200 °C) and isobaric (1 kbar) experiments with a 0.1 N and 3 N HCl and KOH solution, respectively, and one experiment with pure water (series C in Table 2). The infrared spectra of the experimental run products are reproduced in Fig. 6(b), showing that there is a strong pH effect on the zircon–fluid interaction. The absorption intensity increases

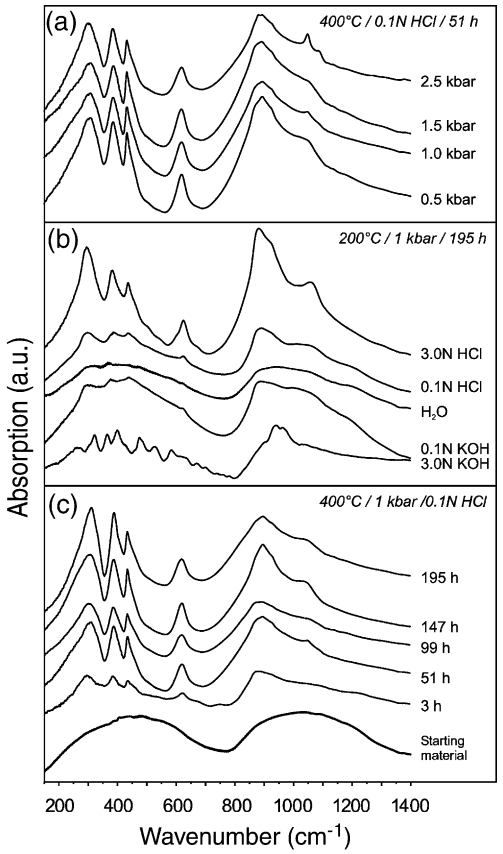

Fig. 6. Stack plot of powder IR absorption spectra between 150 and 1400 cm^{-1} of heavily metamict zircon treated (a) under different fluid pressures, (b) with different solutions and (c) for different periods. The other experimental conditions for each plot are given in the figure. A spectrum from the starting material is shown for comparison in (c).

strongly with increasing HCl concentration in the fluid. When considering the O–Si–O bending mode near 614 cm^{-1}, we notice that the absorption intensity of this mode corresponds to those observed after hydrothermal treatment in 0.1 N HCl at 400 °C (Fig. 3(a)). However, the frequency of this mode is identical within the experimental error to that observed in the 200 °C experiment with 0.1 N HCl and 0.1 N KOH (Fig. 3(b)), suggesting that the short-range ordering process is independent of the pH, but not the amount of recrystallized zircon. A strong signal at 1057 cm^{-1} along with the broad tail at the low frequency side of the zircon Si–O stretching mode at 880 cm^{-1} in the spectrum of the experiment in 3 N HCl suggests that a relative high amount of SiO_2 was produced during the experiment.

Whereas the IR absorption spectra of the run products treated in 0.1 N KOH and 0.1 N HCl solutions are similar, the IR spectrum of the run product treated in an alkaline 3 N KOH solution does not show any remaining characteristic zircon bands, but a high number of new vibrational modes. This clearly indicates that the metamict zircon decomposed during the experiment in strong alkaline solution, which suggests a different alteration mechanism. The reaction product could be identified by X-ray diffraction measurements as a potassium zirconium silicate hydrate (powder diffraction file: 72-1911). Interestingly, crystalline zircon could clearly been detected, in the XRD pattern indicating that either the metamict zircon did not react completely but partly recrystallized or that new zircon re-precipitated from the solution.

3.4. Effect of experimental duration

We designed a set of isothermal experiments running for 3, 51, 99, 147 and 195 h with a 0.1 N HCl at 400 °C and 1 kbar fluid pressure to study the recrystallization kinetics (series D in Table 2). All IR spectra from the run products exhibit extra modes due to ZrO_2 and a silica species (Fig. 6(c)). It is also evident from Fig. 6(c) that the maximum absorption intensity of the zircon bands at 400 °C has already been reached between 3 and 51 h. A longer experimental duration has neither a further significant effect on the absorption intensity nor on the frequency of the zircon bands, implying that a saturation state has been reached. The frequency and the integrated absorption intensity of the bending mode near 614 cm^{-1} of the run product, which was hydrothermally treated for 3 h, are identical within the errors with those obtained from the run product of the experiment at 300 °C, which lasts for 195 h. From this relationship, we can roughly estimate an apparent activation energy, E_a by the 'time to a given fraction' method, which yield an E_a in the order of 1.3 eV. This activation energy is significant lower than those estimated for epitaxial recrystallization under dry conditions, which yield values between 3.3 and 3.8 eV [14–17]. The estimated E_a can be attributed to the recrystallization process, because the solution pH does not affect the solid state transformation process, which is strongly temperature-dependent (see Fig. 3(b)).

3.5. Water incorporation in reacted zircon

The powder absorption IR technique gives no orientational information and does not allow quantitative assessment of the water concentration from hydroxyl stretching bands because only minute difference in the amount of water in the strongly hygroscopic CsI of the sample and the reference pellet could cause erroneous results. We are nevertheless able to comment on some aspects of water incorporation during the zircon–fluid interaction using the powder IR data. Fig. 7 shows representative absorption spectra in the hydroxyl stretching region between 2500 and 4000 cm^{-1}, summarizing

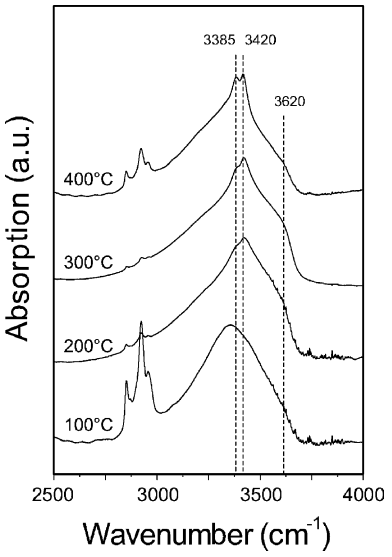

Fig. 7. Stack plot of representative powder IR absorption spectra in the hydroxyl stretching region between 2500 and 4000 cm^{-1} of heavily metamict zircon treated under different temperatures in a 0.1 N HCl solution for 195 h at 1 kbar fluid pressure. Note the formation of two sharp modes at 3385 and 3420 cm^{-1} at fluid temperatures higher than 200 °C, which can be confidently assigned to OH in crystalline zircon. The sharp bands below 3000 cm^{-1} are artifacts of the beam splitter.

the essential features of all experiments. The spectra have been baseline corrected and normalized to show equal maximum absorption intensity so that their shapes may be compared. The starting material and the run products of the 75 °C experiment do not show any signals in the hydroxyl stretching region, which does not mean, due to the limitation mentioned above, that no water is present in the sample. The IR spectrum of the run product of the 100 °C experiment on the other hand shows a single broad water band centered at about 3350 cm^{-1}, which also cannot confidently be assigned to zircon. However, we observe significant different shapes in the hydroxyl stretching region of spectra from run products treated under fluid temperatures of 200 °C and higher. Those spectra, which are characterized by significant water signals, clearly show two sharp additional absorption bands at about 3385 and 3420 cm^{-1} on the top of a broad band. These sharp bands can definitely be assigned to OH in crystalline zircon. They have been detected in natural crystalline and partially metamict zircon crystals [36–38] and have been assigned to be associated with OH sites located at Si-occupied (3385 cm^{-1}) and Si-vacant tetrahedra (3420 cm^{-1}) [36,37]. Since the incorporation of OH at these sites disrupt the local tetrahedral environment, OH may also be responsible for the incomplete recovery of the frequency of the O–Si–O bending mode near 614 cm^{-1} (Fig. 3(b)).

We further note that in the spectra of run products from those experiments, which were carried out at fluid temperatures of 200 °C and higher, the broad OH band is skewed to higher frequencies with a shoulder near 3620 cm^{-1} when compared to the broad water band of the 100 °C experiment. Since SiO_2 was also observed in the run products treated at temperatures below 200 °C experiment, the new OH features must be a result of the hydrothermal treatment and related to OH groups, which are located in the zircon run product. Note that a band at 3620 cm^{-1} has been observed in a transmission IR spectrum ($E\|c$) of a partially metamict zircon from Brevig, Norway [37] and that systematic broad absorption signals near 3560 cm^{-1} appear in single-crystal transmission IR absorption spectra of Sri Lanka zircon samples, which increases in intensity with increasing radiation damage [38]. The spectrum in the hydroxyl stretching region is thus characterized by a superposition of sharp OH signals on a broad OH band, most likely resulting from OH stretching vibrations in crystalline and amorphous regions, respectively. Such superposition has been observed in metamict titanite [39], but to our knowledge not yet in natural zircon. It is also important to mention that a sharp band near 3515 cm^{-1} could not be detected, which has been found in hydroxylated synthetic zircon and which was assigned to a hydrogrossular-type substitution, where $(SiO_4)^{4-}$ is replaced by four $(OH)^-$ groups [40].

4. Discussion

The powder IR absorption spectra of all experiments shown in Figs. 1 and 5 can be understood as reflecting a mixture with variable amounts of amorphous and crystalline zircon, ZrO_2 and a SiO_2 species. In order to investigate the spatial arrangement of these reaction products, we also carried out BSE images of cross-sections from a larger grain from an experiment in 0.1 N HCl at 400 °C and 0.5 kbar fluid pressure. The images show that at 400 °C reaction rims more than 50 μm thick were formed around apparently non-recrystallized zircon (Fig. 8(a)), implying that at 400 °C even the largest grains of the powder used for the experiments must have completely reacted. We could not detect larger inclusions of SiO_2 or ZrO_2 inside the reacted areas by BSE imaging. However, it cannot be ruled out that phase decomposition occurred on a sub-micron scale, as seen in TEM images of heavily metamict zircon that has been annealed under dry conditions at high temperatures [19]. The low apparent activation energy of the recrystallization process may suggest that the formation of recrystallization rims around amorphous zircon was governed by a dissolution–reprecipitation process. However, SiO_2 precipitated at low fluid temperatures, where significant crystallization of $ZrSiO_4$ could not be

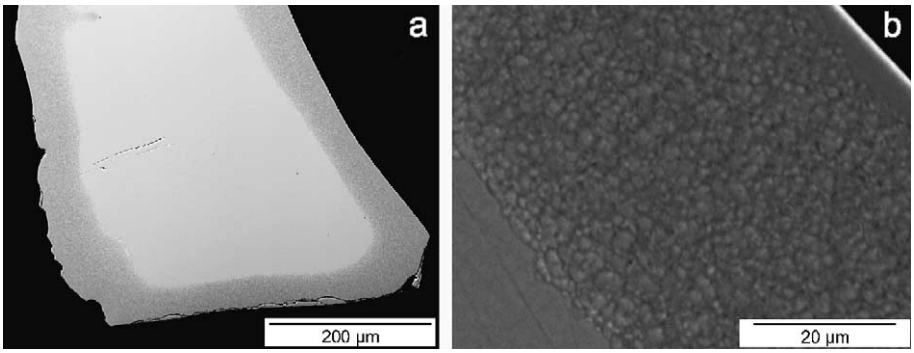

Fig. 8. BSE image of a large grain treated at 400 °C in a 0.1 N HCl for 195 h at 0.5 kbar; (b) shows a magnified section from the sharp interface between the non-recrystallized core (left hand side) and the reaction rim (right hand side). The irregular curved pattern seen in the right BSE image indicates local fluctuations in the chemical composition. Note also that the reaction rim is characterized by a lower average BSE intensity compared with core. See text for further details.

detected as discussed in detail below (Figs. 1 and 3, Fig. 5(b), Table 2). Furthermore, the frequency of the O–Si–O bending mode near 614 cm^{-1} evolves gradually towards the value of crystalline zircon (Fig. 3(b)), which is difficult to explain by a coupled dissolution–reprecipitation model, where crystalline zircon is expected to reprecipitate around an amorphous zircon residue (in such case one would expect the frequency to be that of crystalline zircon in all experiments). It is thus reasonable to suggest that the observed IR signals of crystalline zircon and the reaction-recrystallization zones seen in the BSE images are the result of a diffusion-controlled process. This picture is fully consistent with results from previous hydrothermal experiments with partially metamict zircon [8,22,23].

Recent high-energy molecular dynamic simulations have shown that the displacement cascades directly produced by the heavy recoil during the α-decay event in zircon is characterized by a low density core surrounded by a sphere of densified matter that is partially polymerized [41]. It is the polymerized phase that stabilizes the non-uniform distribution of atoms within the cascade. Diffusion of water into metamict zircon and ion exchange reaction may thus be enhanced inside the depleted matter cores of the amorphous displacement cascades. In such diffusion model, precipitation of ZrO_2 and SiO_2 on the surface of the grains is the result of selective 'leaching' of Zr^{4+} and Si^{4+} from the amorphous domains, which increased the activity of H_4SiO_4 and most likely a $Zr(OH)_{4-n}\,Cl_n^0$ complex in the HCl solution until the equilibrium activities necessary to form the stable oxides are reached. Selective removal of Zr^{4+} and Si^{4+} from the reacted sites could also be detected in previous hydrothermal experiments with partially metamict zircon in acidic solutions [8,22,23]. Leaching of Zr^{4+} and Si^{4+} may be governed by multiple hydrolysis of Si–O–Si linkages as seen in silicate glasses [42], which further opens up the amorphous cascades. Surface dissolution was found to be insignificant under acidic conditions compared with the thickness of the reaction rims as inferred by the still sharp edges of the grains (Fig. 8). However, the mass reduction associated with the leaching reactions and the decrease of the molar volume due to the recrystallization process (see below) have created porosity, which can clearly be seen in Fig. 5(d).

The hydroxylation reactions may be reflected by the formation of the shoulder at about 3620 cm^{-1} at higher fluid temperatures seen in the hydroxyl stretching region (Fig. 7), which indicates the formation of longer and weaker OH bonds [43]. This frequency is similar to 3670 cm^{-1} of OH vibrations in silanol groups of hydrated silica glass [44,45]. One may thus assign the formation of this extra signal at fluid temperatures higher than 200 °C to an increasing amount of new Si–OH groups in the amorphous zircon. On the other hand, an increasing amount of silanol groups was also seen in silica glass with increasing temperature in hydration experiments in water vapor under 0.467 bar pressure [46]. One may thus also assign the signal near 3620 cm^{-1} to hydrated amorphous silica, which precipitated at the surface of the zircon grains (or is located in sub-micron SiO_2 areas inside the non-recrystallized material). Note, however, that this signal is absent in the 100 °C experiment (Fig. 7), although silica bands can clearly be detected in the IR spectrum (Figs. 1 and 2). It is thus more likely that this signal is related to hydroxyl in the amorphous relics.

The strong pH dependence implies that H^+ is the most important species in promoting the reaction. However, in strong alkaline solutions the metamict zircon decomposed, indicating that amorphous zircon dissolved while potassium zirconium silicate hydrate (and possibly zircon) reprecipitated. Such a decomposition of metamict zircon was also observed under hydrothermal conditions in Na_2CO_3 solutions, where a Na–Zr silicate was formed as reaction product [47]. We note, however, that a

hydrothermal treatment in 0.1 N KOH had the same effect on zircon recrystallization as treatment in a 0.1 N HCl solution (Fig. 6(b)). There also appears to be an analogy of the observed pH dependence to those seen in the dissolution behavior of silicate glasses. Under acidic conditions, silicate glass dissolution was found to be controlled by proton-promoted hydrolysis, hydration and ion exchange reactions, whereas under alkaline conditions silica glass dissolves congruently as a result of extensive surface reactions [48].

In addition to the ion exchange reactions, the amorphous material partially recrystallized. It is evident that water (as H^+ or H_2O) must be responsible for the lower apparent activation energy for recrystallization under hydrothermal conditions compared with that determined in dry annealing experiments [14–17]. Such a conclusion is supported by a study on the recrystallization behavior of amorphous strontium titanate in a water vapor environment, which has shown that hydrogen, resulting from the dissociation of water at the surface of the specimen, significantly reduces the activation energy to recrystallization [49]. The small spectral changes near 880 cm^{-1} at temperatures below 200 °C may indicate that recrystallization of the amorphous phase starts already at temperatures below 200 °C. However, it appears more likely that these signals are due to the few disordered crystalline remnants, which were partially recovered during the experiment. Significant recrystallization clearly occurred at temperatures higher than 200 °C, where the absorption intensity of the bending mode near 614 cm^{-1} increases to a level to be significant. This interpretation is further supported by the fact that OH is first seen in an ordered zircon environment at a fluid temperature of 200 °C. Furthermore, Raman measurements on reaction rims formed in experiments on partially metamict zircon with a 2M $AlCl_3$ solution at 175 °C do not show evidence for recrystallization of the amorphous phase at that temperature [22].

The observation that the powder must have already reacted completely at 400 °C seems to contradict with the conclusion that the grains were not fully recrystallized in the high temperature experiments. The isothermal experiments clearly show that the amount of recrystallized zircon after 51 h at 400 °C did not increase anymore at a point, where only about 50% of the amorphous material has been recrystallized (Fig. 6(c)). Furthermore, the isochronal experiments also show a saturation behavior at temperatures higher than 450 °C (Fig. 3). The recrystallization process is initially controlled by the thermodynamic driving force, resulting from the high free energy associated with the transformation of the metastable amorphous state to a stable crystalline state [50]. However, the observed reaction behavior indicates that the activation energy for the recrystallization process abruptly increased after about 50% of the amorphous material had been recrystallized. At this stage the system is controlled by new kinetic constraints because it apparently did not approach the thermodynamic equilibrium anymore. It appears that the thermodynamically metastable amorphous state had been stabilized. Currently, we can only offer a single plausible explanation for this observation, which bases on the diffusion–reaction model given above. After water has infiltrated the metamict network, it first 'catalyzes' recrystallization as reflected by the initially low activation energy for the recrystallization process. However, recrystallized zircon contains some OH, i.e., water is not a catalyst in the strict sense of the term. Nevertheless, it is commonly assumed that crystalline zircon can accommodate only a limited amount of OH in the structure [36–38], at least in an F-free environment [40]. Thus, any excess water had to be expelled from the nucleation sites and the volume occupied by the growing crystalline domains. This increased the water content in the surrounding amorphous regions. With increasing degree of recrystallization, it became eventually energetically impossible to recrystallize the water-rich amorphous domains. At a high concentration of water also partial decomposition of zircon to ZrO_2 and SiO_2 may be preferred compared to the reconstruction of the crystalline lattice. If this is correct, we would expect water-rich amorphous regions to occur next to water-poor crystalline areas. Indeed, BSE images of reacted and recrystallized areas revealed distinct zones of different BSE intensity, which must be attributed to spatial fluctuations of the chemical composition (Fig. 8(b)). Energy-dispersive electron microprobe analysis of these areas revealed Zr–Si ratios close to those of zircon. It is thus tempting to relate these compositional patterns to variations in the water concentration, where the high and low BSE intensity reflects the recrystallized crystalline and residual amorphous regions, respectively.

5. Concluding remarks

Our new results are in full agreement with results from previous hydrothermal experiments with partially, i.e. less radiation-damaged zircon samples [6,22,23]. The reaction between a heavily metamict zircon and an acidic fluid can be best described by a diffusion–reaction model. In such a model, a reaction front is driven by the diffusion of water that promotes ion exchange reactions and 'catalyzes' the recrystallization process. The observed pH dependence of the reaction indicates that the hydronium ion is an important diffusing species. We have shown that at a given temperature the hydronium ion activity in solution governs the velocity of the recrystallization front, i.e. the amount of reacted zircon. However, in an acidic environment the solution pH has no effect on the recovery process itself, which is mainly

controlled by the fluid temperature (see Fig. 3). Only in a 3 N KOH solution the amorphous zircon reacted with KOH and forms potassium zirconium silicate hydrate. This indicates a change in the reaction mechanism, which has to be investigated in more detail in future studies. Recrystallization was found to be activated already at fluid temperatures as low as 200 °C, which is manifested by an apparent activation energy in the order of 1.3 eV. However, we could detect first structural changes in heavily metamict zircon even after hydrothermal treatment at fluid temperatures as low as 75 °C for 195 h, which are believed to be associated with the recovery of highly disordered crystalline remnants. The penetration of water under acidic conditions is associated with selective leaching of Si^{4+} and Zr^{4+}, which precipitated as SiO_2 and tetragonal and monoclinic ZrO_2 on the surface of the grains. The detailed mechanism of such a reaction, which most likely involves hydroxylation of Si–O–Si bonds in the polymerized network of amorphous zircon, is not yet known. It has recently been shown that the recrystallization rate has a strong impact on the hydrothermal stability of U and Th in partially metamict zircon since these elements can easily be incorporated into the newly grown zircon [23]. A detailed investigation of such dependence as a function of the initial degree of radiation damage is critical for a realistic assessment of the long-term stability of plutonium in a potential zircon waste form and is part of ongoing research. We would further like to point out that such alteration behavior may not only be restricted to zircon, but may also be expected in other potential nuclear waste form materials, which can become metamict such as pyrochlore or zirconolite.

A further important observation of the present study was that recrystallization of the amorphous phase was not complete, although the powder used for the experiments has completely reacted. Since crystalline zircon can only accommodate limited amounts of hydroxyl in its structure, any excess water had to be expelled from the recrystallized sites into the amorphous domains, where the increased water content eventually stabilized the amorphous state, i.e. locally hindered zircon crystallization. Such a competition between the 'catalytic' and 'stabilizing' effect of water may thus have caused the coexistence of amorphous and crystalline areas far away from thermodynamic equilibrium. However, it is presently not possible to give a detailed atomistic picture of the competing effect of water on the reaction. We nevertheless speculate here that such conditions may have also produced the variety of curved patterns of self-organization that have been observed as secondary features in natural zircon crystals [51] as well as curved patterns seen in previous hydrothermal experiments with partially metamict zircon [16]. We further hypothesize that such water-rich amorphous material may be extremely unstable once the external water pressure is reduced, which may affect the post-annealing zircon stability. However, further research is necessary to prove these ideas.

Acknowledgements

We would like to thank Christine Putnis for her support during the SEM work, Craig Secker for his help with the hydrothermal experiments, and Jochen Schlüter from the Mineralogical Museum of the University of Hamburg for providing the sample used in the present study. Helpful discussions with Kilian Pollok, Andrew Putnis, and Frank Tomaschek are greatly acknowledged.

References

[1] R.C. Ewing, W. Lutze, W.J. Weber, J. Mater. Res. 10 (1995) 243.
[2] R.C. Ewing, Proc. Nat. Acad. Sci. USA 96 (1999) 3432.
[3] W.J. Weber, Rad. Eff. Def. Solids 115 (1991) 341.
[4] B.E. Burakov, J.M. Hanchar, M.V. Zamoryanskaya, V.M. Garbuzov, V.A. Zirlin, Radiochim. Acta 90 (2002) 95.
[5] K. Högdahl, L.P. Gromet, C. Broman, Am. Mineral. 86 (2001) 534.
[6] T. Geisler, A.A. Rashwan, M.K.W. Rahn, U. Poller, H. Zwingmann, R.T. Pidgeon, H. Schleicher, F. Tomaschek, Min. Mag., in press.
[7] R.C. Ewing, R.F. Haaker, W. Lutze, in: W. Lutze (Ed.), Scientific Basis for Nuclear Waste Management, vol. V, 1982, p. 389.
[8] T. Geisler, M. Ulonska, H. Schleicher, R.T. Pidgeon, W. van Bronswijk, Contrib. Mineral. Petrol. 141 (2001) 53.
[9] T. Murakami, B.C. Chakoumakos, R.C. Ewing, G.R. Lumpkin, R.W.J. Weber, Am. Mineral. 76 (1991) 1510.
[10] W.J. Weber, R.C. Ewing, L.-M. Wang, J. Mater. Res. 9 (1994) 688.
[11] E.K.H. Salje, J. Chrosch, R.C. Ewing, Am. Mineral. 84 (1999) 1107.
[12] I. Farnan, E.K.H. Salje, J. Appl. Phys. 89 (2001) 2084.
[13] M. Zhang, E.K.H. Salje, J. Phys.: Condens. Matter 13 (2001) 3057.
[14] T. Geisler, R.T. Pidgeon, W. van Bronswijk, R. Pleysier, Eur. J. Mineral. 13 (2001) 1163.
[15] T. Geisler, Phys. Chem. Miner. 29 (2002) 420.
[16] A.S. Sandhu, L. Singh, R.C. Ramola, S. Singh, H.S. Virk, Nucl. Instrum. and Meth. B 46 (1990) 122.
[17] A. Meldrum, L.A. Boatner, R.C. Ewing, Mineral. Mag. 64 (2000) 185.
[18] W.J. Weber, J. Am. Ceram. Soc. 76 (1993) 1729.
[19] G.C. Capitani, H. Leroux, J.C. Doukhan, S. Ríos, M. Zhang, E.K.H. Salje, Phys. Chem. Miner. 27 (2000) 545.
[20] M. Zhang, E.K.H. Salje, R.C. Ewing, I. Farnan, S. Ríos, J. Schlüter, P. Leggo, J. Phys.: Condens. Matter 12 (2000) 5189.
[21] F.A. Mumpton, R. Roy, Geochim. Cosmochim. Acta 21 (1961) 217.
[22] T. Geisler, R.T. Pidgeon, W. van Bronswijk, R. Kurtz, Chem. Geol. 191 (2002) 141.

[23] T. Geisler, R.T. Pidgeon, R. Kurtz, W. van Bronswijk, H. Schleicher, Am. Mineral., in press.
[24] A. Putnis, Min. Mag. 66 (2002) 689.
[25] T. Geisler, H. Schleicher, Chem. Geol. 163 (2000) 269.
[26] S. Ríos, E.K.H. Salje, M. Zhang, R.C. Ewing, J. Phys.: Condens. Matter 12 (2000) 2401.
[27] M. Zhang, E.K.H. Salje, M.A. Carpenter, I. Parsons, H. Kroll, S.J.B. Reed, A. Graeme-Barber, Am. Mineral. 82 (1997) 849.
[28] P. Dawson, M.M. Hargreave, G.R. Wilikinson, J. Phys. C 4 (1971) 240.
[29] C. Pecharroman, M. Ocana, C.J. Serna, J. Appl. Phys. 80 (1996) 3479.
[30] C.M. Phillippi, K.S. Mazdiyasni, J. Am. Ceram. Soc. 54 (1971) 254.
[31] C. Carlone, Phys. Rev. B 45 (1992) 2079.
[32] C. Jégou, S. Gin, F. Larché, J. Nucl. Mater. 280 (2000) 216.
[33] T.A. Guiton, C.G. Pantano, Colloids Surf. A 14 (1993) 33.
[34] M. Sitarz, M. Handke, W. Mozgawa, Spectrochim. Acta A 56 (2000) 1819.
[35] M. Tomozawa, D.-L. Kim, A. Agarwal, K.M. Davis, J. Non-Cryst. Solids 288 (2001) 73.
[36] J.A. Woodhead, G.R. Rossman, L.T. Silver, Am. Mineral. 76 (1991) 1533.
[37] L. Nasdala, A. Beran, E. Libowitky, D. Wolf, Am. J. Sci. 301 (2001) 831.
[38] M. Zhang, E.K.H. Salje, R.C. Ewing, J. Phys.: Condens. Matter 14 (2002) 3333.
[39] M. Zhang, G.A. Lee, E.K.H. Salje, A. Beran, Am. Mineral. 86 (2001) 904.
[40] R. Caruba, A. Baumer, M. Ganteaume, P. Iacconi, Am. Mineral. 70 (1985) 1224.
[41] K. Trachenko, M. Dove, E.K.H. Salje, Phys. Rev. B 65 (2002) 180102R.
[42] B.C. Bunker, J. Non-Cryst. Solids 179 (1994) 300.
[43] E. Libowitzky, Monatsh. Chem. 130 (1999) 1047.
[44] M.L. Hair, J. Non-Cryst. Solids 19 (1975) 299.
[45] A.J. McMillan, R.K. Remmele, Am. Mineral. 71 (1986) 772.
[46] K.M. Davis, M. Tomozawa, J. Non-Cryst. Solids 185 (1995) 203.
[47] N.G. Rizvanova, O.A. Levchenkov, A.E. Belous, N.I. Bezmen, A.N. Maslenikov, A.N. Komarov, A.F. Makeev, L.K. Levskii, Contrib. Mineral. Petrol. 139 (2000) 101.
[48] P.V. Brady, W.A. House, in: P.V. Brady (Ed.), Physics and Chemistry of Mineral Surfaces, CRC, New York, 1996, p. 249.
[49] T.W. Simpson, I.V. Mitchell, J.C. McCallum, L.A. Boatner, J. Appl. Phys. 76 (1994) 2711.
[50] S. Ellsworth, A. Navrotsky, R.C. Ewing, Phys. Chem. Miner. 21 (1994) 140.
[51] R.T. Pidgeon, A.A. Nemchin, G.J. Hitchen, Contrib. Mineral. Petrol. 132 (1998) 288.